LA-UR- 99-5103

Title: RESIDUAL STRESS MEASURMENT AND PREDICTION IN
A HARDENED STEEL RING

Author(s): Michael B. Prime, ESA-EA
Vincent C. Prantil, Sandia Livermore
Partha Rangaswamy, MST-8
Felix P. Garcia, MST-7

Los Alamos
NATIONAL LABORATORY

Residual Stress Measurement and Prediction in a Hardened Steel Ring

M. B. Prime[1], V. C. Prantil[2], P. Rangaswamy[1] and F. P. Garcia[1]

[1] Los Alamos National Laboratory, Los Alamos, NM, USA
[2] Sandia National Laboratories, Livermore, CA, USA

Abstract. The residual stress profile in a hardened layer of steel was measured and then compared with a finite element prediction. A thick ring made of low alloy gear steel was case hardened by carburization and quenching. The residual hoop stress variation in the 1 mm thick hardened layer was measured using the crack compliance method, in which surface strains are measured as an axial slot is incrementally extended from the outer surface inward using wire electric discharge machining (EDM). The surface residual stresses were also measured using x-ray diffraction. The results compared very well with finite element predictions using DANTE, a heat treatment simulation software package interfacing with the finite element code ABAQUS. The heat treatment cycle is simulated in an uncoupled serial analysis of carburization by diffusion, quenching by conduction and convection including phase transformation kinetics, and finally a structural analysis incorporating TRansformation-Induced Plasticity (TRIP). Accurate residual stress profiles require detailed knowledge of the heat transfer coefficients of the quench media as well as alloy-dependent descriptions for phase transformation kinetics and TRIP strains.

Introduction

The process of carburization followed by quenching is widely applied to steels. It produces a surface layer with both increased hardness for wear resistance and compressive residual stresses for fatigue resistance. Unfortunately, such treatment can also produce distortion and internal quench and fatigue cracks. The furnace and quench schedules produce complex thermal histories in which parts experience thermal expansion and contraction simultaneously along with phase transformations which introduce significant volume changes. The complex interaction and relative timing of these competing factors determine the residual stresses and distortion.

In the past, attempts to model the effects of phase transformations have met with mixed success. Empirical methods of incorporating a temperature dependent yield strength to simulate a phase change do not account for the volume change or any additional plasticity [1,2]. Mimicking the phase change with large changes in the thermal expansion coefficient can capture the effects of the spherical volume change but not the accompanying microplasticity [1,3,4]. Calculations which account for the dilatational volume change explicitly, but not the microscopic deviatoric strains, exhibit large discrepancies with measured residual stresses [1,5,6,7,8]. Properly accounting for the coupling between the thermal, mechanical, and microstructural mechanisms is crucial for accurately predicting the residual stresses and distortions. In particular, modeling the microstructural phase transformations and path-dependent material behavior is critical.

Because of the complexity of developing a predictive model, experimental validation is essential. However, measurement of residual stresses in a relatively thin (~1 mm) hardened layer is difficult. On a specimen similar to the one measured in this paper, neutron and x-ray diffraction measurements encountered several difficulties [9]. The neutron diffraction measurements required a complicated analysis because the carbon gradient resulted in a strong variation in the stress free lattice spacing. It was also difficult to achieve the required spatial resolution. The x-ray

measurements failed to show the tensile interior stresses required to balance the compressive surface stresses. This was postulated to be caused by accumulation of errors from the layer removal process used to give a depth profile.

Mechanical, or relaxation, methods offer several advantages for measuring residual stresses in heterogeneous materials. Unlike with diffraction methods, multiple phases, texture, and microstress variations have negligible effects on macrostress measurements. However, there are other difficulties. The layer removal and sectioning methods lack the spatial resolution required for the thin hardened layer in this study [10]. Measurements with the hole-drilling method would require special care because of the possibility of introducing stresses during machining of hardened steel [11]. The method used in this study, the crack compliance method, gives excellent spatial resolution of stresses and uses electric discharge machining, which cuts even the hardest materials with ease.
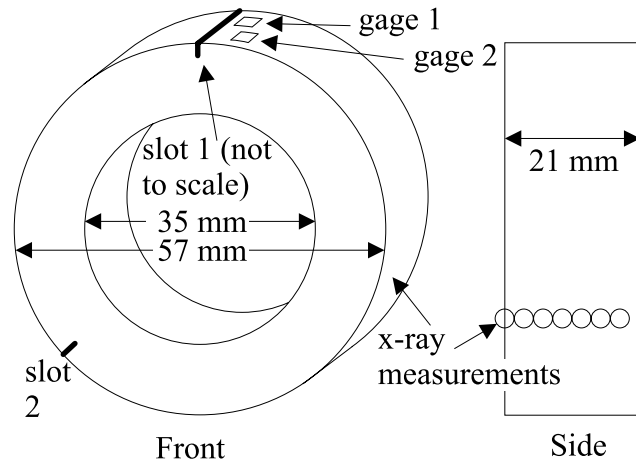
Figure 1. Specimen size and measurement locations.

Specimen Preparation

A 0.2% carbon content steel ring, Fig. 1, was carburized using a boost-diffuse cycle for 3.25 hours at 900 $^{\circ}$C and then at 840 $^{\circ}$C for 0.75 hours, to form a carbon content of 0.85 wt. % at the surface. The ring was quenched in molten salt for 4 minutes with its axis vertical, followed by air cooling to room temperature. Finally, the ring was tempered at 177 $^{\circ}$C for 1.5 hours.

Measurements

Crack Compliance. The crack compliance method [12,13] involves incrementally introducing a slot into a part containing residual stress. Strain gages on appropriate surfaces measure strain at each increment of slot depth. These measured strains are used to solve for the original residual stresses. This method has successfully profiled residual stress variation with depth in surface regions as thin as 100 μm [14] and through parts as thick as 166 mm [15]. The primary advantage of the crack compliance method is its excellent spatial resolution. It can also easily measure the stress intensity factor caused by a crack in a residual stress field [16].

Residual stress variation with depth is determined from the measured strains using a series expansion approach [17]. The unknown residual stresses are written as a series expansion,

$$\sigma_\theta(r) = \sum_{i=1}^n A_i P_i(r), \tag{1}$$

where the A_i are unknown coefficients, the P_i are some functional series, and r is the slot depth direction, which for this ring is the radial direction measured from the outer surface in. Then for each term in the series the strain that would be measured at the strain gage location, the compliance function C_i, is calculated. Using superposition, the strains for the Eq. 1 stresses can be written as

$$\varepsilon_\theta(r) = \sum A_i C_i(r). \tag{2}$$

Finally, a least-squares fit is performed between the measured strains and those given by Eq. 2, resulting in the coefficients A_i and, hence, the stresses from Eq. 1. The least squares fit makes this inversion procedure very tolerant of noise and errors in the strain measurements.

On the surface of the ring, thermally compensated strain gages with gage lengths of 0.81 mm were mounted so that one gage would be as close as possible to the cut and the other would be about 1 mm farther away, see Fig. 1. A quarter-bridge circuit was used to read the strains. A slot was made in 100 μm depth increments using wire electric discharge machining (wire EDM) while the specimen was submerged in 20° C de-ionized water. The machine was set for a fine surface finish to minimize the recast layer. A 50 μm diameter tungsten wire was used for cutting the first slot and made a slot about 89 μm wide. The cutting was stopped when the wire broke at 1.35 mm depth. The strains measured during this test are shown in Fig. 2. A second cut was made at a set of gages 120° circumferentially away from the first cut using a larger wire, a 100 μm diameter zinc-coated wire, in order to cut deeper. The 110 μm wide slot was stopped at 2.8 mm depth when the strain reading began to level off.

Figure 2. Strains measured during cutting of first slot and fit given by Eq. 2.

The stresses were expressed (Eq. 1) as a Fourier series to improve the stability of the fit near the domain endpoints, which is a commonly observed problem with polynomial expansions [13]. The compliance functions were calculated using a numerical solution for a finite-width rectangular slot in a semi-infinite medium [18]. The actual slot has a round bottom, but this has no effect on the compliances for the gage locations used in these tests [19]. Approximating the curved ring as locally flat is acceptable because the maximum slot depth (2.8 mm) is small compared to the radius of curvature (28.5 mm). All of the measured strains were used in the least squares fit except the first few measured by the more distant gage because of their low magnitude. The strains given by Eq. 2 after the fit are shown in Fig. 2 for the first cut. Errors in the stress prediction are estimated using a Monte Carlo analysis and used to select the appropriate expansion order [20]. A four-term Fourier series was optimal for the shallow cut, and eight terms were used for the deeper cut.

The use of wire EDM to measure residual stress has been extensively studied [12]. Analysis revealed no EDM effect on our measurements of the ring. This is probably because we used a "fine surface finish," or "skim cut," setting. It may also have resulted from using new anti-electrolysis power source, which is supposed to improve the integrity of the machined surface.

X-ray. Residual hoop stresses were measured along the axial direction on the outer ring surface (see Fig. 1) for comparison with crack-compliance measurements and model predictions. The residual stresses were determined using the classical x-ray (d vs. $\sin^2\psi$) diffraction technique [21] and a diffracting plane (222) in the high angle region of $2\theta \approx 137^o$. These measurements were made using a Huber stress goniometer with X-rays generated from an 18 kW Scintag rotating anode and Cu radiation (wavelength ≈ 1.54Å). A 3 mm diameter collimator was used, and the distance from the sample surface to the tip of the collimator was 40 mm. Stresses were mapped at seven positions across the surface using an increment of 3 mm. Measurements in positive and negative ψ tilts confirmed that shear stresses were not present. The ψ angles ranged from 0 to 60° in increments of 15°. The average stress from the six measurement points in the central region of the surface, which were fairly constant, was compared with the crack compliance measurements and the model.

Modeling

The modeling strategy adopted here couples differential equations for phase evolution with a multiphase macroscopic state variable material model. The state variable model is based on a
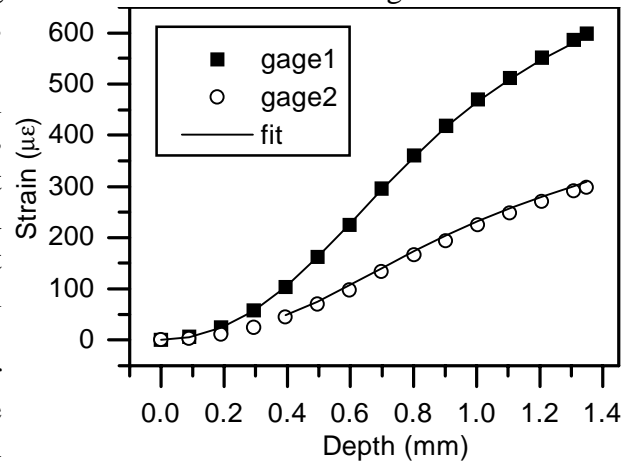
mixture theory wherein we characterize the mechanical behavior of individual phases and sum their behavior to obtain the macroscopic response [22,23]. This elastic-plastic constitutive behavior of the individual phases is highly nonlinear [24]. The reader is referred to Prantil et al. [22] for details beyond what is covered below and to Denis [25] for a review of phase transformation interactions.

The hypoelastic stress rate, an objective Jaumann rate, is related through Hooke's law to the elastic strain rate:
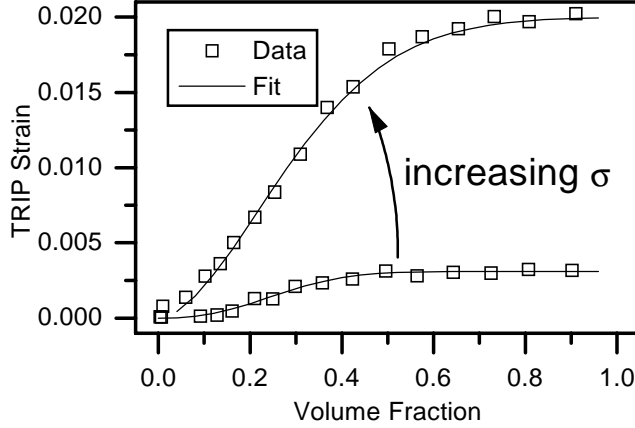
Figure 3. TRIP strain development during

$$\overset{o}{\sigma} = \mathcal{L} : \dot{\varepsilon}^e = \mathcal{L} : \left(\dot{\varepsilon} - \dot{\varepsilon}^p - \dot{\varepsilon}^{TRIP} \right). \qquad (3)$$

The plastic strain rate is determined at the phase level and then summed over all phases to obtain the macroscopic rate. The hardening behavior depends on the carbon content, temperature and strain rate. Phase interactions are accounted for by introducing a trans-formation induced plasticity (TRIP) strain rate,

$$\dot{\varepsilon}^{TRIP} = \frac{Am}{B} \left(\frac{\phi}{B} \right)^{m-1} \exp\left(-\left(\frac{\phi}{B} \right)^m \right) |\sigma'| \dot{\phi} , \qquad (4)$$

that accounts for variations in phase properties and transformation volume change [26,27,28,29]. Here, ϕ is the volume fraction of product phase. Transformation strains are both temperature and carbon dependent. The integrated TRIP strain varies sigmoidally with volume fraction as shown in Fig. 3. In low carbon steels, this integrated contribution to the strain is significant; i.e. it approaches the order of the dilatational thermal strains when the deviatoric stress components exceed 100 MPa. For this application, Eq. 4 has been fit to data obtained from quench dilatometer specimens under compressive loading. The deviatoric stress is the proportionality constant coupling the TRIP strain rate to the transformation rate

This model is joined with a new approach to simulating phase transformation kinetics [30]. The kinetic rate equations for each product phase are derived using a thermodynamic formulation and fit to experimental data. Below, the volume fraction of austenite, ferrite, pearlite, bainite and martensite are denoted by Φ_a, Φ_f, Φ_p, Φ_b, and Φ_m respectively. The temperature is given by θ and the carbon concentration by C. A fundamental balance results in the following system of equations for phase evolution which couples naturally to the differential equations governing the mechanical and thermal analyses of the quench history:
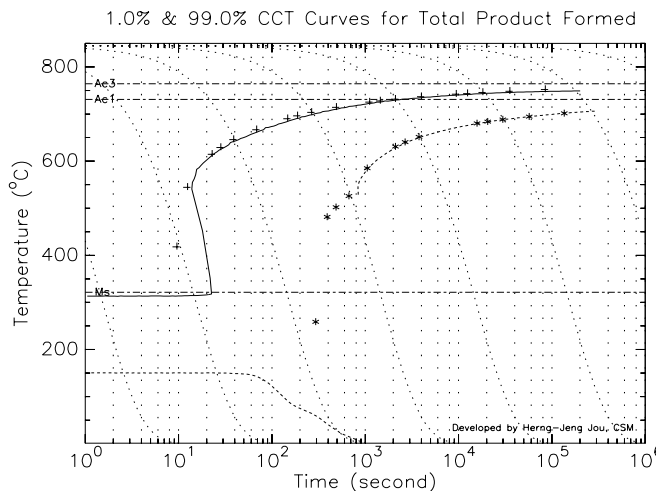
Figure 4. Predicted and measured CCT curves.

$$\frac{d\Phi_f}{dt} = v_f(C,\theta) \Phi_f^{\alpha_f} \Phi_f^{\beta_f} \left\{ \Phi_{f,final}(C,\theta) - \Phi_f \right\}$$

$$\frac{d\Phi_{p,b}}{dt} = v_{p,b}(C,\theta) \Phi_{p,b}^{\alpha_{p,b}} \Phi_{p,b}^{\beta_{p,b}}$$

$$\frac{d\Phi_m}{dt} = \begin{cases} 0; & \theta > M_s(C), \\ -v_m(C,\theta) \Phi_m^{\alpha_m} \Phi_m^{\beta_m}; & \theta < M_s(C) \end{cases} \qquad ,(5)$$

$$\Phi_{f,p,b,m}(0) = 0.0001$$

$$\Phi_a = \left(1 - \Phi_f - \Phi_p - \Phi_b - \Phi_m \right)$$

where the functions $v(C,\theta)$ as well as the α and

β constants are material dependent quantities that are determined for each material using time temperature transformation (TTT), continuous cooling transformation (CCT) data, and by studying the influence of stress on the kinetics through compression and tension experiments. An example of a typical CCT prediction is shown in Fig. 4.

This work addresses application of the constitutive model, DANTE, developed for the Heat Treatment Distortion Project (HTDP) at the National Center for Manufacturing Sciences (NCMS) [31]. Under this program, an extensive series of tests were performed to fit both the single phase plasticity [32] and transformation kinetics models. These models have been implemented as a User Material (UMAT) Interface to the ABAQUS finite element code [33].

The axisymmetric finite element mesh of the ring specimen consisted of 380 quadrilateral elements with finer discretization used near the carburized case. The ABAQUS four-node linear displacement element CAX4 was used for the mechanical analysis and the corresponding heat transfer and mass diffusion element DCAX4 was used for the carburization and thermal analyses. The calculated carbon profile was in excellent agreement with the carbon concentration measured to approximately 1 mm depth using a microprobe [31]. Thermal boundary conditions were obtained by applying measured surface temperatures to a finite element model and computing surface heat fluxes which are then converted to an equivalent set of surface heat transfer coefficients. The resulting thermal field is provided as input to the mechanical analysis.

Results & Discussion

The calculated residual hoop stress profile near the outer surface is compared with the measured values in Fig. 5. The agreement is good just below the surface and relatively insensitive to a finer mesh discretization. The upturn in the measured profile near the surface may be due to surface decarburization or auto tempering during the air cool, neither of which is currently modeled. These explanations are supported by hardness measurements, which show a similar upturn. Given these qualifications, the shape of the residual stress profile and correlation of measured and predicted values are excellent.

Figure 5. Measured residual hoop stress and FEM model prediction. Depth is taken from the outer diameter inwards.

The crack compliance method measures only the depth variation in the residual stresses. Some assumptions are implicitly made about the stress variation along the slot length, in this case the axial direction. It has been shown that the measured strains are primarily affected by the residual stresses axially within eight times the slot depth of the strain gage [34]. The X-ray and model results confirm that the stresses can be considered constant within that range. The waviness in the tensile stress profile measured at large depths is an artifact of fitting the entire depth range with a single series expansion. A splined polynomial approach [35,36] could improve this at the expense of increased computational effort.

The crack compliance method has proven to be an ideal method for measuring residual stresses in this hardened steel specimen.

References

[1] J. A. Goldak: Recent Trends in Welding Science and Technology, eds. S.A. David and M. Vitek, (Gatlinburg, TN: ASM International, 1990), 71-82.

[2] D. Dubois, J. Devaux, and J. B. Leblond: Proc. Fifth Int. Conf. on Pressure Vessel Tech., Vol. 2, Materials and Manufacturing (San Francisco, CA: ASME, 1984), 1210-1239.

[3] S. Sjöström: Mater. Sci. & Tech., **1** (1985), 823-829.

[4] J. A. Goldak et al.: Proc. Int. Symp. on Computer Modeling of Fabrication Processes and Constitutive Behavior of Metals, (Ottawa, Canada 1986).

[5] A. S. Oddy, J. A. Goldak, and J. M. J. McDill: J. Pressure Vessel Tech., **114** (1992), 33-38.

[6] B. L. Josefson and C. T. Karlsson: J. Pressure Vessel Tech., **114** (1992), 376-378.

[7] A. S. Oddy, J. A. Goldak, and J. M. J. McDill: Eur. J. Mech. A/Solids, **9** (1990), 253-263.

[8] J. A. Goldak et al.: Proc. of the IUTAM Symposium, (Lulea, Sweden 1991), 1-31.

[9] M. A. M. Bourke et al.: Mater. Sci. & Engng., **A257** (1998), 333-340.

[10] J. Lu, M. James, and G. Roy: *Handbook of Meas. of Residual Stresses* (Fairmont Press, 1996).

[11] A. Niku-Lari, J. Lu, and J.F. Flavenot: Exp. Mech., **25** (1985), 175-185.

[12] W. Cheng, I. Finnie, M. Gremaud, and M. B. Prime: J. Engng. Mater. Tech., **116** (1994), 1–7.

[13] M. B. Prime: Appl. Mech. Reviews, **52** (1999), 75-96.

[14] W. Cheng, et al.: J. Engng. Mater. Tech., **116** (1994), 556–560.

[15] W. Cheng and I. Finnie: Eng. Fract. Mech., **46** (1993), 79–91.

[16] H. J. Schindler, W. Cheng, and I. Finnie: Exp Mech, **37** (1997), 272-277.

[17] G. S. Schajer: J. Engng. Mater. Tech., **103** (1981), 157–163.

[18] W. Cheng and I. Finnie: J. Engng. Mater. Tech., **115** (1993), 220–226.

[19] D. Nowell: J Strain Anal. Engng Design, **34** (1999), 285-294.

[20] W. Y. Lin: Thesis, Univeristy of California, Davis (1999).

[21] I. C. Noyan and J. B. Cohen: *Residual Stress, Measurement by Diffraction and Interpretation*, (Springer-Verlag, New York, 1987).

[22] V. Prantil, M. L. Callabresi, G. S. Ramaswamy, J. Lathrop, M. Lusk: J. Engng. Mater. Tech. (submitted).

[23] D. Bammann et al.: ASM Quenching and Distortion Conference Proceedings, eds. G. Totten, M. Howes, S. Sjostrom, and K. Funatani (1996), 367.

[24] D. J. Bammann et al.: NUMIFORM'95: The Fifth International Conference on Numerical Methods in Industrial Forming Processes, (Ithaca, New York 1995), 215-218.

[25] S. Denis: J. Physique IV, **6** (1996), 159-174.

[26] J. B. Leblond, G. Mottet, and J. C. Devaux: J. Mech. Phys. Solids, **34** (1986), 395-409.

[27] J. B. Leblond, G. Mottet, and J. C. Devaux: J. Mech. Phys. Solids, **34** (1986), 411-432.

[28] J. B. Leblond, J. Devaux, and J. C. Devaux: Int. J. Plasticity, **5** (1989), 551-572.

[29] J. B. Leblond, J. Devaux, and J. C. Devaux: Int. J. Plasticity, **5** (1989), 573-591.

[30] M. Lusk, G. Krauss, and H.-J. Jou, J. de Physique IV, **C8** (1995) 279-284.

[31] Phase I Project Summary Report, NCMS Project "Predictive Model & Methodology for Heat Treatment Distortion", January 1994 - December 1997.

[32] J. F. Lathrop, "BFIT - A Program to Analyze and Fit the Sandia Plasticity (BAMMANN) Model Parameters to Experimental Data," Sandia National Laboratories Report SAND97-8218.

[33] *ABAQUS User's Manual V5.7,* Hibbitt, Karlsson and Sorensen ,Pawtucket, RI (1998).

[34] W. Cheng, I. Finnie, and Ö. Vardar: J. Engng Mater. Tech., **113** (1991), 199-204.

[35] M. Gremaud, W. Cheng, I. Finnie, M. B. Prime: J. Engng. Mater. Tech., **116** (1994), 550–555.

[36] G. Petrucci and B. Zuccarello: J. Strain Anal. Engng Des., **33** (1998), 27-37.

Correspondence: prime@lanl.gov